Article

J. Biol. Regul. Homeost. Agents. 2024; 38(6): 5217–5228
https://doi.org/10.23812/j.biol.regul.homeost.agents.20243806.417

Exploring the Anti-Osteosarcoma Effects and Mechanisms of Rhizoma Paridis Total Saponins Based on SLC7A11-Mediated Ferroptosis

Qian Tan[1,2,3], Dae-jung Yang[4,*]

[1]Orthopedic Department, The Affiliated Children's Hospital of Xiangya School of Medicine, Central South University (Hunan Children's Hospital), 410000 Changsha, Hunan, China
[2]Hunan Provincial Key Laboratory of Pediatric Orthopedics, 410000 Changsha, Hunan, China
[3]The School of Pediatrics, University of South China, 410000 Changsha, Hunan, China
[4]Graduate School of Sehan University Department of Physical Therapy, Sehan University, 58447 Mokpo City, Jeollanam-do, Republic of Korea
*Correspondence: pt6226@sehan.ac.kr (Dae-jung Yang)
Submitted: 25 February 2024 Revised: 3 April 2024 Accepted: 7 April 2024 Published: 1 June 2024

Background: Rhizoma paridis total saponins (RPTS) constitute the principal bioactive compound in *Rhizoma paridis*, demonstrating anticancer properties in various tumor types. However, its mechanism of action in osteosarcoma (OS) remains unclear. This study aimed to elucidate the role of RPTS on OS cells and tumor progression, focusing on its modulation of Solute Carrier Family 7 Member 11 (SLC7A11)-mediated ferroptosis.

Methods: 143B cells were cultured *in vitro*, and assays were conducted to assess cell viability, proliferation, apoptosis, migration, intracellular reactive oxygen species (ROS) levels, mitochondrial membrane potential, ferroptosis-related proteins, and epithelial-mesenchymal transition (EMT) markers. Nude mice were subcutaneously injected with 143B cells to establish an osteosarcoma mouse model. Tumor volume and weight were recorded. EMT process markers and ferroptosis-related protein expression were detected in the tumor tissues.

Results: *In vitro* experiments revealed that RPTS significantly inhibited cell viability, proliferation, and migration and promoted apoptosis ($p < 0.05$). Moreover, RPTS increased intracellular ROS accumulation and reduced mitochondrial membrane potential ($p < 0.05$). RPTS inhibited the EMT process, upregulated p53 protein expression, and downregulated glutathione peroxidase 4 (GPX4) and SLC7A11 expression in 143B cells ($p < 0.05$). Overexpression of SLC7A11 rescued RPTS-induced ROS accumulation and ferroptosis in 143B cells ($p < 0.05$), and significantly increased RPTS-induced inhibition of cell proliferation and migration ($p < 0.05$). *In vivo*, RPTS significantly suppressed tumor growth and EMT markers, upregulated p53 protein expression and decreased GPX4 and SLC7A11 protein expressions ($p < 0.05$).

Conclusion: RPTS induced ferroptosis in osteosarcoma by inhibiting SLC7A11 expression and regulated cell viability, proliferation, apoptosis, migration, and EMT processes, demonstrating an inhibitory effect on osteosarcoma.

Keywords: Rhizoma paridis total saponins; osteosarcoma; SLC7A11; ferroptosis; EMT

Introduction

Osteosarcoma (OS), a malignant tumor arising from bone tissue, is characterized by tissue heterogeneity, local invasion, and rapid infiltration and dissemination. Predominantly affecting children and teenagers, OS often metastasizes early, primarily in non-skeletal tissues such as the lungs [1]. Despite the adoption of surgery combined with chemotherapy as the standard treatment regimen, the 5-year survival rate remains low, ranging from 60% to 75% in non-metastatic cases, with less than 20% survival among patients with metastases [2,3]. Common first-line chemotherapeutic agents include adriamycin (ADR), cisplatin (DDP), and high-dose methotrexate (MTX). Although the 5-year survival rate for individuals diagnosed with osteosarcoma has grown to approximately 60% due to recent advancements in diagnostic techniques and the adoption of surgery in combination with neoadjuvant chemotherapy, numerous patients are compelled to discontinue their treatment due to challenges such as chemotherapy resistance, severe side effects, high recurrence rates, and expensive treatment costs [4]. Hence, there is an urgent need to explore alternative anti-tumor strategies and drugs with low side effects, high safety profiles, and affordability.

Metastasis constitutes a critical step in tumor progression, involving the migration of malignant cells from the primary site to distant normal tissues [5]. For successful metastasis, tumor cells must acquire migratory and invasive properties, which are closely associated with epithelial-mesenchymal transition (EMT) [6]. EMT is the process through which cells become more mesenchymal and lose

Journal of
BIOLOGICAL REGULATORS
and Homeostatic Agents

their epithelial characteristics. One accurate indicator of the progression of EMT is the downregulation of the epithelial marker Epithelial-cadherin (E-cadherin), which is correlated with the overexpression of certain mesenchymal markers, like vimentin and Neural-cadherin (N-cadherin). EMT is linked to OS onset, progression, and lung metastases, according to mounting data [7]. Moreover, in clinical settings, EMT promotes the emergence of tumor stem cells, driving metastatic spread and conferring resistance to therapy [8]. These findings underscore the potential of inhibiting or reversing the EMT as a promising strategy to mitigate OS metastasis and recurrence.

In recent years, ferroptosis has emerged as a focal point in numerous studies on tumor therapy, garnering considerable attention from scholars as a novel direction in tumor therapy. Ferroptosis represents a distinct form of cell death characterized by iron-dependent phospholipid peroxidation, distinguishing it from conventional programmed cell death mechanisms such as apoptosis, necrosis, and autophagy. Fundamentally, ferroptosis is initiated by the iron-dependent accumulation of reactive oxygen species (ROS), leading to lipid peroxidation. Morphologically, cells undergoing ferroptosis manifest a rounded shape, accompanied by decreased mitochondrial volume, reduced or absent mitochondrial cristae, disrupted outer mitochondrial membranes, and lack of nuclear or chromatin condensation [9].

Numerous studies have demonstrated the critical role of Solute Carrier Family 7 Member 11 (SLC7A11) in regulating ferroptosis in OS. Elevated expression of SLC7A11 enhances cystine absorption, thereby protecting tumor cells from undergoing ferroptosis and experiencing oxidative stress overload through increased glutathione (GSH) synthesis. Consequently, SLC7A11 is recognized as a pivotal protein in the regulation of ferroptosis [10]. Luo *et al*. [11] demonstrated the inhibitory effect of Bavachin on MG63 and HOS osteosarcoma cell lines. Bavachin regulates ferroptosis in osteosarcoma cells through the STAT3/p53/SLC7A11 axis. Bavachin-induced cell death can be reversed by iron chelators, antioxidants, and ferroptosis inhibitors. Additionally, it has been observed that the clinical drug sorafenib indirectly inactivates glutathione peroxidase 4 (GPX4) by inducing intracellular cystine deficiency and reducing GSH synthesis following System Xc- inhibition, thereby facilitating ferroptosis in tumor cells [12]. Collectively, these findings underscore the potential of elucidating the ferroptosis mechanism in developing cancer therapeutic strategies.

Rhizoma paridis total saponins (RPTS) are steroidal saponins isolated from the rhizome of the plant and are the primary active constituents of *Rhizoma paridis*. In recent years, the anticancer potential of RPTS has garnered significant attention, with associated mechanisms encompassing inhibition of tumor cell growth, promotion of apoptosis, suppression of tumor metastasis, and enhancement of chemosensitivity, among other pathways [13]. A study demonstrated that A549 cells were incubated with RPTS combined with JNK inhibitor SP600125 for 48 hours. RPTS not only decreased the expression of SLC7A11 and GPX4 in the cells but also markedly raised cellular ferroptosis resistance, encouraged the build-up of ROS and Malondialdehyde (MDA) in the cells, and stimulated the JNK/p53 pathway to induce cellular ferroptosis [14]. Another investigation revealed that Rhizoma paridis saponin could modulate and upregulate the expression of Divalent Metal Transporter 1 (DMT1) and Transferrin Receptor 1 (TFR1) in triple-negative breast cancer cells, disrupting cellular iron homeostasis. GPX4 expression was also reduced. In addition, by promoting p53 expression and inhibiting SLC7A11 expression, cystine transporter was blocked, affecting the synthesis of glutathione. Consequently, this led to the accumulation of lipid peroxides and reactive oxygen species, facilitating the initiation of the cellular ferroptosis program [15]. In the present study, we investigated the effects of RPTS on ferroptosis and OS tumor growth using 143B cells and implanted nude mice as research subjects. Our findings indicate that RPTS induces SLC7A11-mediated ferroptosis, which promotes OS cell apoptosis while inhibiting proliferation and migration. These findings highlight new avenues for RPTS research in the management of OS.

Materials and Methods

Reagents and Instruments

Reagents: Rhizoma paridis total saponins (RPTS, A1701, MUST Bio-technology Co., Ltd., Chengdu, China); Ferrostatin-1 (Fer-1, HY-100579, MedChemExpress, Monmouth Junction, NJ, USA); DMEM-high glucose medium, 100× penicillin/streptomycin mixture, RPMI-1640 complete medium, 0.25% trypsin-EDTA solution, phosphate buffer solution (PBS), cell cryopreservation tubes (11965-092, 15140122, 11875093, 25200072, AM9624, 374080, Gibco, Shanghai, China); 4% paraformaldehyde, 3-4,5-dimethylthiazol-2yl 2,5-diphenyltetrazolium bromide (MTT), crystal violet, dimethyl sulfoxide (DMSO) (P1110, M8180, C8470, D8371, Solarbio, Beijing, China). Cell culture dishes, 24-well plates with 8.0 μm Transwell chambers (706001, 702011, NEST, Wuxi, China). RIPA lysis buffer, fetal bovine serum (P0013B, C0232, Beyotime, Shanghai, China). Instruments: BD Accuri C6 flow cytometer (Becton Dickinson, Franklin Lake, NJ, USA); DYY-7C electrophoresis instrument (Liuyi Biotechnology Company Limited, Beijing, China); IX73 inverted fluorescence microscope imaging system (Olympus, New York, NY, USA); enzyme labeling instrument (LumiStation 1800Plus, Molecular Devices, Silicon Valley, CA, USA); centrifuge (TD4Z-WS, Sigma, St. Louis, CA, USA); image analysis software Image J (V1.8.0.112, NIH, Madison, WI, USA); protein blotting system (ProteinSimple, Bio-Rad, Hercules, CA, USA).

Cell Cultures

The human osteosarcoma cell line 143B (CRL-8303, ATCC cell bank, Shanghai, China) was utilized. Cells were cultured in DMEM high-glucose medium supplemented with 10% FBS, 1% penicillin, and streptomycin, and maintained at 37 °C with 5% CO_2 in a humidified atmosphere. The cells were routinely passaged using 0.25% trypsin solution when they reached 80% to 90% confluence. Cells in the logarithmic growth phase were harvested for subsequent experiments. Prior to the experimentation, cells were tested for mycoplasma and confirmed to be mycoplasma-free. All adhered to aseptic techniques to prevent cell contamination. Furthermore, the cells underwent STR validation.

Cell Grouping and Processing

Cells were randomly divided into Control, RPTS-L, M, H, and Fer-1+RPTS-H groups. The Control group received an equal volume of DMSO. Cells in the low (L), medium (M), and high (H) dosage groups were treated with 2, 4, and 6 μg/mL RPTS, respectively. In the Fer-1+RPTS-H group, cells were treated with 6 μg/mL RPTS for 1 hour, followed by the addition of 5 μmol/mL Fer-1 to continue the treatment. To further investigate whether RPTS induces ferroptosis through SLC7A11, cells were randomly divided into the Control, RPTS-H, oeSLC7A11, and oeSLC7A11+RPTS-H groups. The oeSLC7A11 and oeSLC7A11+RPTS-H groups were transfected with the overexpression plasmid before treatment with 6 μg/mL RPTS.

Transfection of SLC7A11 Overexpression Plasmid

OS cells were cultured to 80–90% confluence, then harvested, centrifuged, and resuspended in a complete medium. Subsequently, cells were seeded at a density of 120,000 cells per well into six-well plates. After the cells reached 50% confluence, transfection was performed. Lipofectamine 3000 (Invitrogen, Shanghai, China) and overexpression (Vigene Biosciences, Shanghai, China) solutions were prepared in a serum-free medium, mixed after a 10-minute incubation period, and then incubated for 15 minutes. The cell culture medium was replaced with a serum-free medium, and the transfection complex was added, followed by incubation for 48 hours. Plasmids were procured from Cloud Ark Bioscience Co. (Guangzhou, China). The coding sequence of the SLC7A11 overexpression plasmid is provided in the **Supplementary Material**.

MTT Assay for Cell Viability

143B cells were seeded at a density of 5000 cells/well in 96-well plates and allowed to adhere for 24 hours. Following adherence, cells were treated according to the experimental groups and further incubated for 12, 18, and 24 hours. Subsequently, 20 μL of 5 mg/mL 3-4,5-dimethylthiazol-2yl 2,5-diphenyltetrazolium bromide (MTT) solution was added, and the plates were incubated for 4 hours. Following incubation, the culture medium was removed, and 150 μL of DMSO was added to each well, followed by a 20-minute incubation. Absorbance at 490 nm was measured using an enzyme marker.

Determination of Cell Migration Capacity

143B cells were seeded in 6-well plates until reaching 80% to 90% confluence. Subsequently, a sterile 10 μL pipette tip was used to create a scratch on the cell monolayer. Following scratching, cells were washed with PBS, treated according to the experimental groups, and the initial scratch width at 0 hours was recorded. Subsequently, the scratch widths at the same positions were observed and recorded at 24 hours. The healing rate of scratches in each group was calculated to assess the lateral migration ability of 143B cells.

Cells, at 80% confluence, were trypsin-digested, suspended in a serum-free medium, and inoculated at a density of 3×10^4 cells per chamber. In the lower chamber of a 24-well plate, 10% serum medium was added based on the experimental groups. After 24 hours of incubation, the chambers were removed from the plate. Cells were washed with PBS three times for 3 minutes each, stained with 0.1% crystal violet for 15 minutes, and subsequently washed with PBS once and purified water twice. Group labels were applied to the chambers, followed by drying and microscopic photography to assess the longitudinal migration capacity of 143B cells.

Plate Cloning Assay for Cell Proliferation

Cells were cultured until 80% confluence, then trypsin-digested, resuspended in a medium, and gradient-diluted to a density of 500–1000 cells/mL. Subsequently, the cells were seeded into six-well plates, and after adherence, the old medium was discarded. Cells were then treated according to the experimental groups and incubated for 24 hours. Following this, the cells were replenished with fresh complete medium and continued incubation for 7 days, with medium replacement every 2–3 days. The number and status of clone formation were observed using a microscope. The culture medium was then aspirated and discarded, and the cells were washed three times with PBS buffer. Fixation was performed using 4% paraformaldehyde for 20 minutes, followed by staining with 0.1% crystal violet solution for 15 minutes. Subsequently, the cells were washed three times with PBS, air-dried, and photographed to assess clone formation.

Measurement of Apoptosis

Cells were washed twice with cold PBS and resuspended in 250 μL binding buffer. Then, 100 μL of the cell suspension was transferred to a 5 mL flow tube. Following the experimental procedure outlined in the instruction manual for the apoptosis detection kit (C1062S, Beyotime,

Journal of
BIOLOGICAL REGULATORS
and Homeostatic Agents

Shanghai, China), 5 µL of Annexin V-FITC and 5 µL of PI liquid were added for double-staining. The staining process was conducted in the dark for 20 minutes. Subsequently, flow cytometry was used to detect the cells.

Determination of ROS

143B cells were collected for digestion, and the cells were seeded in 24-well cell culture plates at a cell density of 5×10^5 cells/mL. After cell attachment, treatment based on the assigned groups was administered. The medium was discarded, and cells were washed with PBS before resuspension. For intracellular degreasing, 2 µmol/L DCFH-DA (S0033M, Beyotime, Shanghai, China) was added to each group of cells, followed by incubation at 37 °C for 20 minutes. After removal of the loading solution, cells were further incubated with PBS for 0.5 hours to ensure thorough intracellular degreasing. Subsequently, cells were washed with PBS and detected using flow cytometry.

Measurement of Mitochondrial Membrane Potentials

Cells were treated according to the assigned groups, washed with PBS, and collected. 500 µL of cell suspension was transferred into a centrifuge tube, centrifuged for 5 minutes, and the supernatant was removed. Mitochondrial membrane potential probe JC-1 (C2006, Beyotime, Shanghai, China) was added, and cells were incubated for 60 minutes at 37 ℃. Following the incubation, cells were washed with PBS, resuspended, and immediately subjected to flow cytometry for detection.

Western Blotting (WB)

Tumor tissues and cells from the treated groups were lysed and homogenized using a cold RIPA lysis solution for 30 minutes. Protein concentration in the samples was quantified using the BCA Protein Assay Kit (P0012S, Beyotime, Shanghai, China). Subsequently, proteins were mixed with an up-sampling buffer (P0015, Beyotime, Shanghai, China) and denatured in boiling water for 5 minutes. 40 µg from each protein sample was loaded onto an SDS-PAGE gel (P0012A, Beyotime, Shanghai, China), transferred to a PVDF membrane (FFP36, Beyotime, Shanghai, China), and blocked with 5% skimmed milk powder (P0216-300 g, Beyotime, Shanghai, China).

Primary antibodies against SLC7A11 (AF7992, 1:1000, Beyotime, Shanghai, China), GPX4 (AF7020, 1:1000, Beyotime, Shanghai, China), p53 (AF0255, 1:1000, Beyotime, Shanghai, China), Matrix Metalloproteinase-2 (MMP-2, A19080, 1:500, Abclonal, Wuhan, China), Matrix Metalloproteinase-9 (MMP-9, A25299, 1:500, Abclonal, Wuhan, China), Neural-cadherin (N-cadherin, A3045, 1:500, Abclonal, Wuhan, China), Epithelial-cadherin (E-cadherin, A3044, 1:500, Abclonal, Wuhan, China), and GAPDH (AF1186, 1:1000, Beyotime, Shanghai, China) were applied, and the membrane was incubated overnight at 4 °C. Subsequently, the membrane was incubated with a secondary antibody HRP-labeled goat anti-rabbit IgG (H+L) (A0208, 1:2000, Beyotime, Shanghai, China) at room temperature for 2 hours. Following a 5-minute wash in TBST solution, BeyoECL Star (P0018AS, Beyotime, Shanghai, China) was applied for detection for 30 seconds. *GAPDH* served as an internal reference, and Image J software (V1.8.0.112, NIH, Madison, WI, USA) was used to quantify the intensity of the bands.

Animal Modeling and Grouping

The investigations began with a week-long acclimation period for male BALB/c nude mice (4–6 weeks, 16–18 g, Hunan SJA Laboratory Animal Co., Ltd., Changsha, China). To establish an osteosarcoma mouse model, the nude mice were subcutaneously injected with 1×10^7/mL 143B cells into the right abdomen [16]. Tumor-bearing nude mice, consisting of six individuals in each of three groups (Control, RPTS, and RPTS+Fer-1), were selected four weeks post-inoculation and randomly assigned, with three mice in each group. A dose of 135 mg/kg RPTS was administered by gavage to the RPTS and RPTS+Fer-1 groups once a day, while Fer-1 (2 mg/kg) was intraperitoneally injected into the RPTS+Fer-1 group once a day. The Control group received saline for two weeks. Successful modeling was confirmed by achieving a tumor volume of approximately 1000 mm^3 within 30 days [17]. Subsequently, all mice were euthanized via carbon dioxide asphyxiation. Tumor tissues were collected and divided into two portions, one fixed in 4% paraformaldehyde and the other cryopreserved at –80 ℃.

Immunohistochemistry

Tumor tissue sections were rinsed in PBS buffer, subjected to thermoantigenic repair, and then treated with 10% goat serum (C0265, Beyotime, Shanghai, China) for 20 minutes. Subsequently, primary antibodies against SLC7A11 (AF7992, 1:200, Beyotime, Shanghai, China), GPX4 (AF7020, 1:200, Beyotime, Shanghai, China), and p53 mouse monoclonal antibody (AF0255, 1:200, Beyotime, Shanghai, China) were applied dropwise and incubated for 12 hours at 4 °C. The sections were rinsed with 1% PBS, followed by the application of secondary antibodies horseradish peroxidase-labeled goat anti-rabbit IgG (H+L) (A0208, 1:200, Beyotime, Shanghai, China) and a 15-minute incubation. After staining with DAB solution (P0202, Beyotime, Shanghai, China), hematoxylin (G1080, Solarbio, Beijing, China) was used for re-staining. Subsequently, the sections were dehydrated, made transparent, dried, sealed, and photographed for observation.

Statistical Analysis

The experimental data were expressed as mean ± standard deviation ($\bar{x} \pm$ SD). Data analysis was performed using SPSS 22.0 (IBM Corp., Armonk, NY, USA). Two-

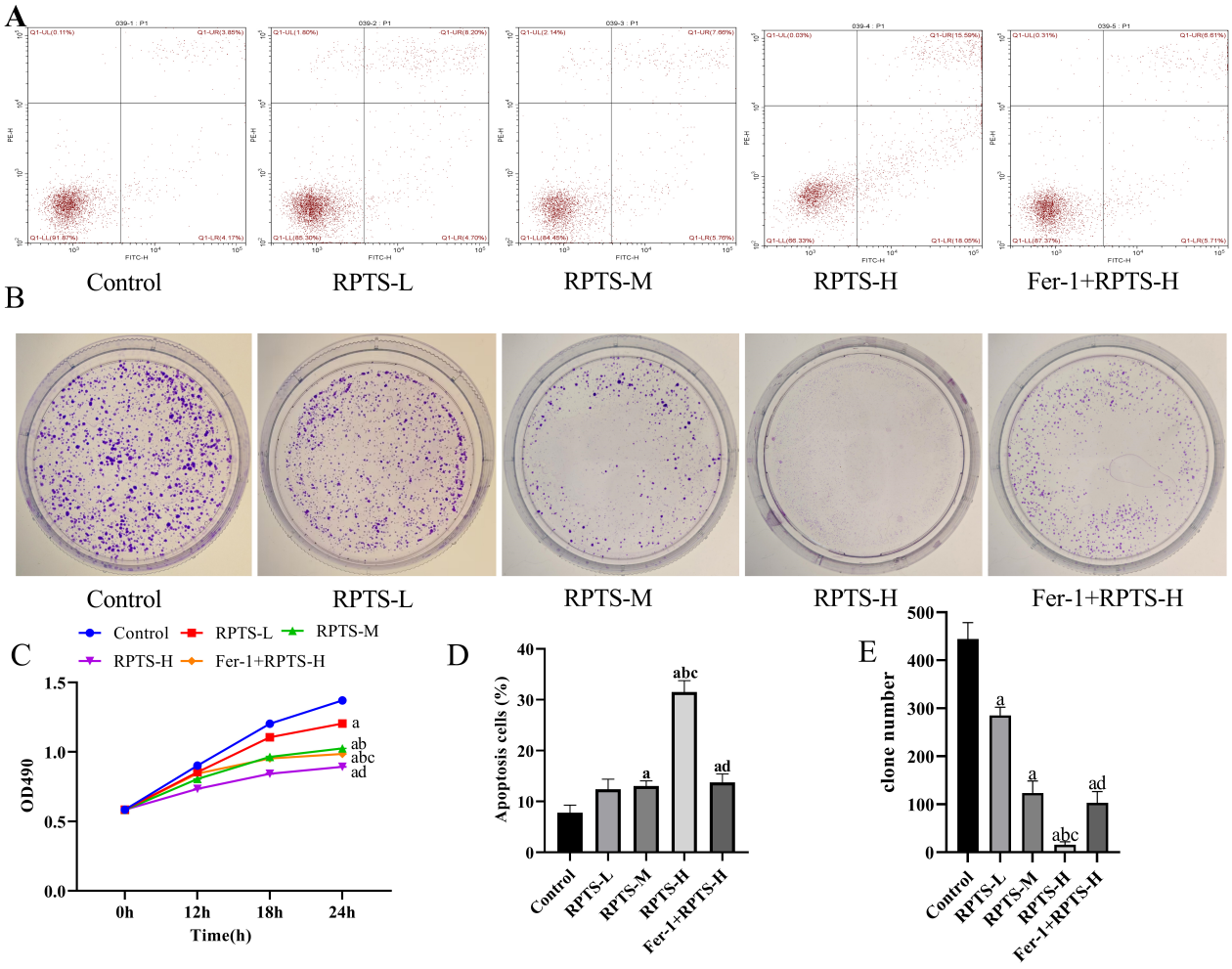

Fig. 1. Rhizoma paridis total saponins (RPTS) reduces OS cell viability and proliferation while promoting apoptosis. (A,D) Cell apoptosis was evaluated by flow cytometry. (B,E) Cell proliferation was examined by plate colony formation assay. (C) Cell viability was assessed by MTT assay. $^{a}p < 0.05$ vs Control, $^{b}p < 0.05$ vs RPTS-L, $^{c}p < 0.05$ vs RPTS-M, $^{d}p < 0.05$ vs RPTS-H. RPTS-L, M, H, rhizoma paridis total saponins-low, -middle, -high; Fer-1, Ferrostatin-1; OS, osteosarcoma; MTT, 3-4,5-dimethylthiazol-2yl 2,5-diphenyltetrazolium bromide. n = 3.

group comparisons were conducted using the *t*-test, while comparisons across multiple groups were made using analysis of variance (ANOVA). Post hoc comparisons were performed using the sequential Bonferroni test for data with significant differences. Statistical significance was set at $p < 0.05$.

Results

RPTS Reduces OS Cell Viability and Proliferation and Promotes Apoptosis

Administration of RPTS led to a significant decrease in cell viability, reduced cell proliferation, and increased apoptosis compared to the Control group (Fig. 1, $p < 0.05$). The addition of Fer-1 significantly reversed these effects compared to the RPTS-H group (Fig. 1, $p < 0.05$). These findings suggest that RPTS reduces viability and proliferation while promoting apoptosis by inducing ferroptosis in 143B cells.

RPTS Inhibits the Migratory Ability of OS Cells and Regulates EMT Marker Expression

The results of the cell scratch healing assay and Transwell assay revealed that RPTS treatment significantly reduced the cell scratch healing rate and the number of migrated cells compared to the Control group (Fig. 2A,B. $p < 0.05$). The addition of Fer-1 notably reversed these effects, surpassing those of the RPTS-H group (Fig. 2A,B. $p < 0.05$). Western blotting was employed to assess the expression of EMT process markers. Compared to the Control group, the results indicated that RPTS treatment significantly increased E-cadherin protein expression while de-

Journal of
BIOLOGICAL REGULATORS
and Homeostatic Agents

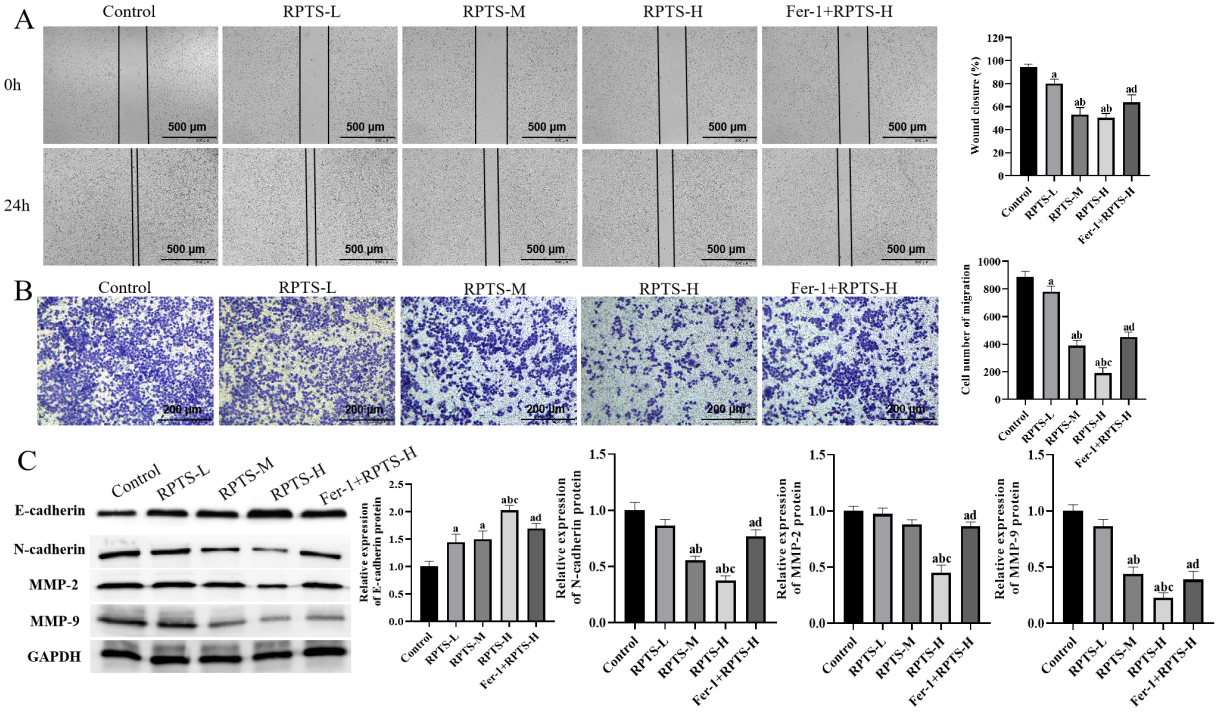

Fig. 2. RPTS inhibits the migratory capability of osteosarcoma cells and modulates the expression of EMT markers. (A) Wound healing assay (scale bar = 500 μm). (B) Transwell chamber assay (scale bar = 200 μm). (C) Analysis of EMT process markers using western blotting. $^{a}p < 0.05$ vs Control, $^{b}p < 0.05$ vs RPTS-L, $^{c}p < 0.05$ vs RPTS-M, $^{d}p < 0.05$ vs RPTS-H. E-cadherin, Epithelial-cadherin; N-cadherin, Neural-cadherin; MMP-2, Matrix Metalloproteinase-2; MMP-9, Matrix Metalloproteinase-9; EMT, epithelial-mesenchymal transition. n = 3.

creasing N-cadherin, MMP-2, and MMP-9 protein expression (Fig. 2C. $p < 0.05$). Compared with the RPTS-H group, the addition of Fer-1 significantly reversed these effects (Fig. 2C. $p < 0.05$). These findings suggest that RPTS inhibits cell migration and regulates the expression of EMT-related markers in 143B cells.

Effect of RPTS on Ferroptosis-Related Protein Expression, Mitochondrial Membrane Potential and ROS Levels in OS Cells

As indicated by flow cytometry, RPTS was observed to significantly elevate ROS levels and decrease mitochondrial membrane potential compared to the Control group (Fig. 3A,B. $p < 0.05$). The addition of Fer-1 yielded significantly different outcomes compared to the RPTS-H group (Fig. 3A,B. $p < 0.05$). Furthermore, western blotting was employed to investigate the expression of ferroptosis markers. The results demonstrated that RPTS administration significantly increased the expression of p53 protein while concurrently decreasing the expression of GPX4 and SLC7A11 proteins compared to the Control group (Fig. 3C. $p < 0.05$). The addition of Fer-1 led to markedly different results compared to the RPTS-H group (Fig. 3C. $p < 0.05$). These findings suggest that RPTS enhances the oxidative stress response of osteosarcoma cells and induces ferroptosis.

Overexpression of SLC7A11 Alleviates Ferroptosis in OS Cells Induced by RPTS

The SLC7A11 overexpression plasmid was used to transfect 143B cells to validate whether RPTS induced ferroptosis in osteosarcoma cells through SLC7A11. Results demonstrated that SLC7A11 overexpression rescued RPTS-induced cell death in 143B cells (Fig. 4A. $p < 0.05$). Moreover, the upregulation of SLC7A11 attenuated the inhibition of proliferation and migration caused by RPTS administration (Fig. 4B,C. $p < 0.05$). Additionally, SLC7A11 overexpression mitigated RPTS-induced ROS accumulation (Fig. 4D. $p < 0.05$). Notably, SLC7A11 overexpression rescued the reduction in GPX4 and SLC7A11 protein expression induced by RPTS and increased p53 protein expression (Fig. 4E. $p < 0.05$). These findings indicate that SLC7A1 overexpression inhibits RPTS-induced ferroptosis in 143B cells, suggesting a close relationship between RPTS-induced ferroptosis and SLC7A11.

Impact of RPTS on Tumor Growth and EMT Process

To evaluate the effect of RPTS on tumor growth *in vivo*, nude mice were injected with 143B cells to induce tumor formation, allowing assessment of RPTS function *in vivo*. In nude mice, RPTS therapy dramatically slowed down the growth of tumors in response to the DMSO group,

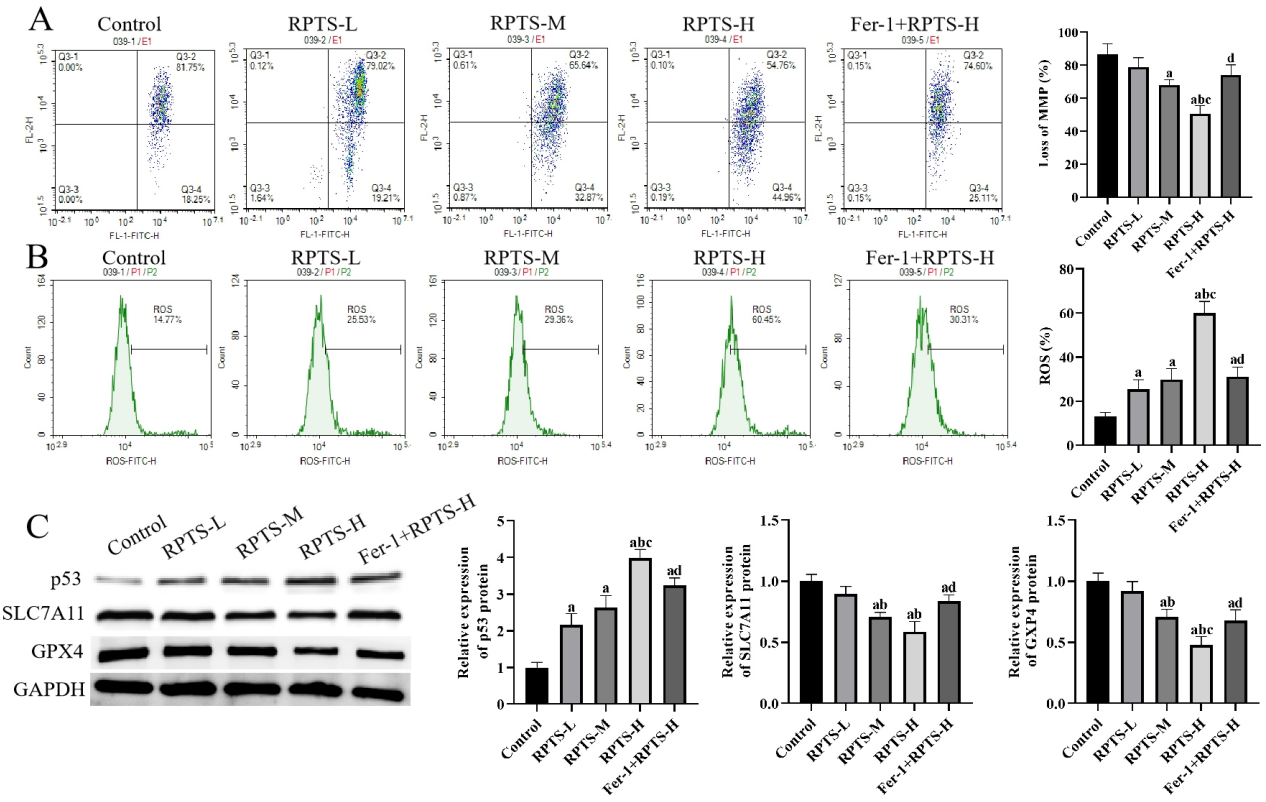

Fig. 3. Effects of RPTS on the expression of ferroptosis-related proteins, mitochondrial membrane potential, and ROS expression in OS cells. (A) Measurement of mitochondrial membrane potential. (B) Determination of ROS activity. (C) Analysis of ferroptosis-related protein expression levels using western blotting. $^{a}p < 0.05$ vs Control, $^{b}p < 0.05$ vs RPTS-L, $^{c}p < 0.05$ vs RPTS-M, $^{d}p < 0.05$ vs RPTS-H. GPX4, glutathione peroxidase 4; SLC7A11, Solute Carrier Family 7 Member 11; ROS, reactive oxygen species. n = 3.

but the addition of Fer-1 reversed this effect (Fig. 5A–C. $p < 0.05$). Further examination of EMT-related markers in tumor tissues revealed that the RPTS treatment markedly increased E-cadherin protein expression while significantly reducing N-cadherin, MMP-2, and MMP-9 protein expression compared to the DMSO group. However, this effect was reversed upon the addition of Fer-1 (Fig. 5D–H. $p < 0.05$). These findings suggest that RPTS inhibits tumor growth *in vivo* by inducing ferroptosis while regulating the EMT process.

Impact of RPTS on Ferroptosis-Related Proteins p53, SLC7A11, and GPX4 in Tumor Tissues

Western blotting and immunohistochemistry analyses revealed that RPTS administration significantly elevated p53 protein expression in OS tissues while concurrently reducing levels of GPX4 and SLC7A11 proteins compared to the DMSO group (Fig. 6. $p < 0.05$). This effect was reversed upon the addition of Fer-1, a ferroptosis inhibitor. These findings suggest that RPTS induces ferroptosis in osteosarcoma tumors.

Discussion

Osteosarcoma (OS), a malignant tumor, predominantly affects children, teenagers, and young adults. While early detection combined with timely surgery and chemotherapy has improved survival rates, the adverse effects of current chemotherapeutic agents remain a significant challenge, often leading to a poor prognosis for patients. Consequently, there is an urgent need to develop new chemotherapeutic agents with fewer adverse effects to address this clinical dilemma [18].

In recent years, the anticancer properties of traditional Chinese medicines have garnered attention [19]. One advantage of these medicines is that they have fewer side effects than traditional chemotherapeutic treatments. Rhizoma paridis' primary active component is RPTS. Through its direct effect on various cancer cell lines, RPTS has been demonstrated in recent studies to be able to inhibit tumor growth. The mechanisms underlying this effect include the regulation of multiple signaling pathways, related protein expression, inhibition of tumor cell proliferation, induction of programmed tumor cell death, and inhibition of tumor cell invasion and metastasis [20].

Journal of
BIOLOGICAL REGULATORS
and Homeostatic Agents

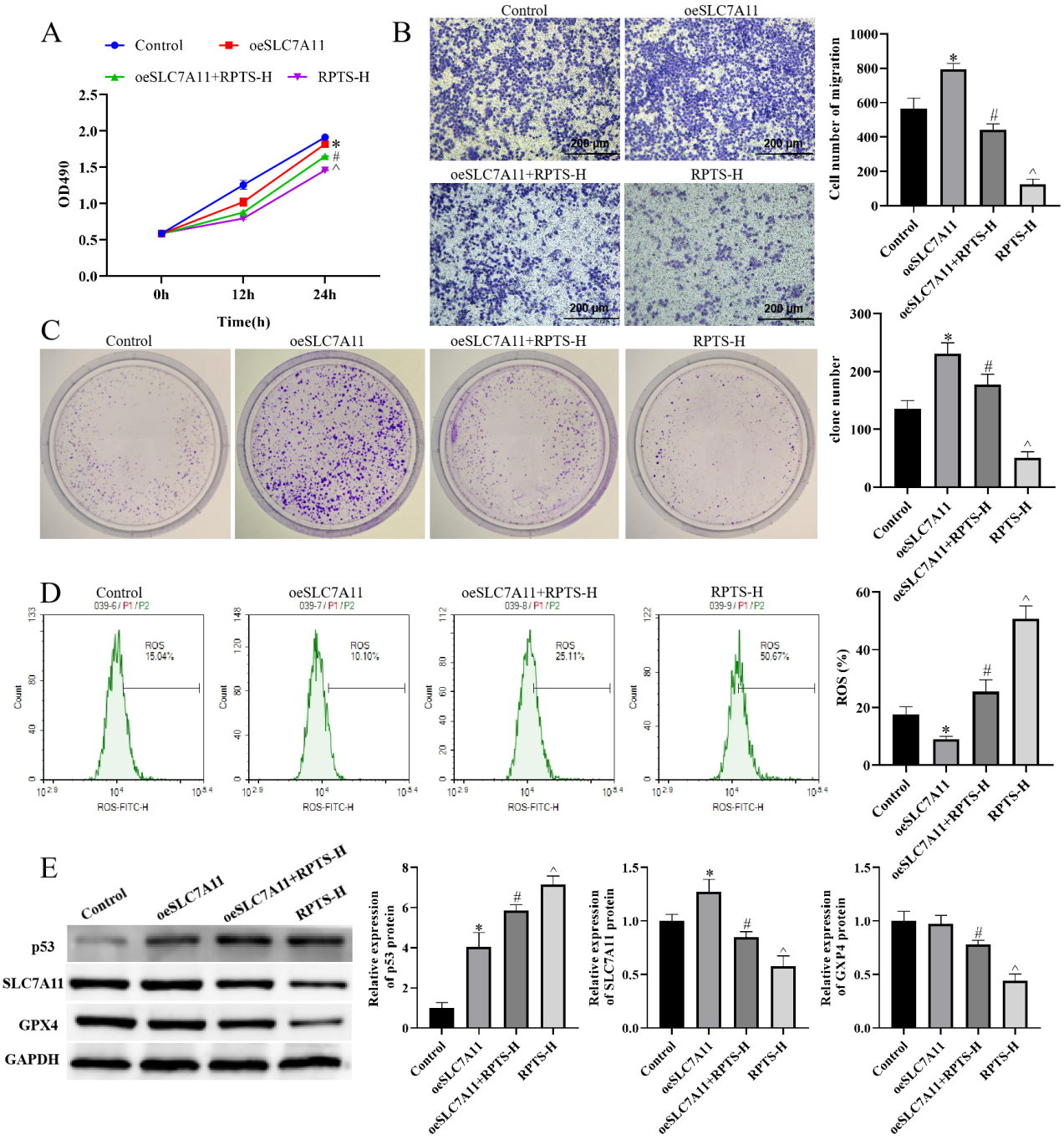

Fig. 4. Overexpression of SLC7A11 alleviates RPTS-induced ferroptosis in OS cells. (A) Cell viability was assessed by MTT assay. (B) Transwell chamber assay for cell migration (scale bar = 200 μm). (C) Cell proliferation was examined by plate colony formation assay. (D) Determination of ROS activity. (E) Analysis of ferroptosis-related protein expression using western blotting. *$p < 0.05$ vs Control, $^{\#}p < 0.05$ vs oeSLC7A11, $^{\wedge}p < 0.05$ vs oeSLC7A11+RPTS-H. n = 3.

Our study found that RPTS significantly reduced the viability and proliferation of 143B cells while promoting apoptosis in *in vitro* experiments. It was also observed in *in vivo* experiments that RPTS significantly inhibited tumor growth and this effect was reversed by the addition of Fer-1, suggesting that RPTS may regulate the biological behavior of 143B cells and tumor growth by inducing ferroptosis.

EMT describes the morphological transition of epithelial cells towards a mesenchymal phenotype. Throughout this transformation, epithelial cells actively diminish the cell-cell adhesion system, relinquish their polarity, and adopt a mesenchymal phenotype characterized by decreased intercellular interactions and heightened migratory capabilities [21]. Tumor cells undergoing EMT can en-

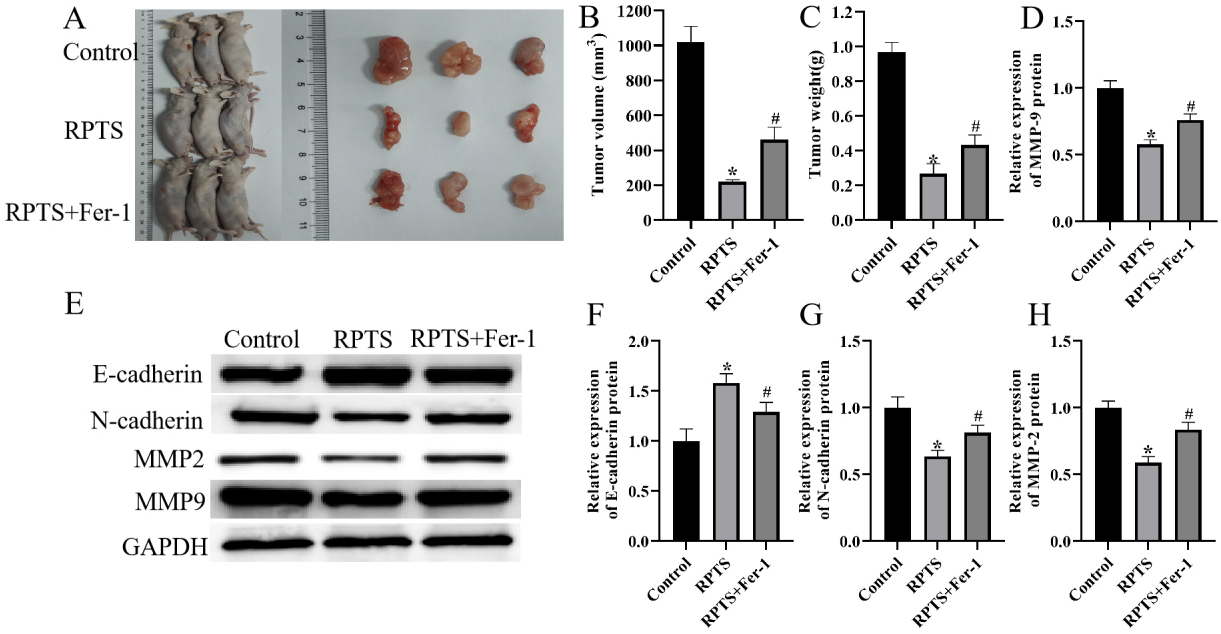

Fig. 5. Effects of RPTS on tumor growth and the EMT process. (A–C) *In vivo* measurement of tumor growth. (D–H) Analysis of EMT process markers using western blotting. *$p < 0.05$ vs Control, #$p < 0.05$ vs RPTS. n = 3.

hance their ability to infiltrate vascular endothelium and enter the circulation, underscoring the significance of EMT in conferring invasive and metastatic properties to malignant cells.

Matrix metalloproteinases (MMPs) are zinc-dependent endopeptidases responsible for the degradation of extracellular matrix (ECM), thereby facilitating various cellular processes. MMPs are pivotal in promoting angiogenesis, aiding tumor cell invasion, and fostering metastasis by modulating ECM dynamics. In EMT, MMPs regulate tumor cell interactions by cleaving E-cadherin, thereby enhancing tumor cell invasion and metastasis [22]. Notably, Matrix Metalloproteinase-2 (MMP-2), a principal member of the MMP family, disrupts the basement membrane, promoting local and distant infiltration of tumor cells, and is pivotal in promoting tumor cell invasion and metastasis. Similarly, Matrix Metalloproteinase-9 (MMP-9), a member of the gelatinase family, plays a multifaceted role in angiogenesis, metastasis, and cancer invasion [23,24].

In this study, we observed that RPTS treatment inhibited the migratory capacity of osteosarcoma cells and regulated the EMT process by upregulating E-cadherin expression while downregulating the protein levels of N-cadherin, MMP-2, and MMP-9 in a concentration-dependent manner. Meanwhile, *in vivo* experiments also verified this result. All the above results were reversed after Fer-1. These results suggest that RPTS can inhibit cell migration and invasion by suppressing the EMT process in osteosarcoma cells, and ferroptosis may be a potential mechanism of action of RPTS to inhibit tumor metastasis and invasion.

Ferroptosis represents a distinct form of cell death initiated by iron-dependent phospholipid peroxidation. Its unique regulatory mechanism involves three key biological features: intracellular ferrous ion concentration overload, GPX4 inactivation, and lipid ROS accumulation. The SLC7A11/GPX4 axis shields cells from iron death [25]. SLC7A11, a vital constituent of the xCT transporter, is vital for cystine uptake and glutamate efflux. Cystine undergoes intracellular reduction to cysteine, contributing to glutathione (GSH) synthesis facilitated by GSH synthase [26]. GSH, a reduced substrate for GPX4, is a pivotal cofactor for GPX4 to exert its antioxidant function. p53, a tumor suppressor protein, suppresses tumor cells by triggering ferroptosis [11]. Jiang *et al.* [27] observed that p53 induces ferroptosis by negatively regulating SLC7A11, thereby inhibiting cystine transport. In a study by Lin *et al.* [28], the curcumin analog EF24 significantly elevated lipid peroxide levels, iron concentration, and ROS levels in osteosarcoma cells, inducing cell death by suppressing GPX4 expression through the regulation of HMOX1. Similarly, gambogenic acid induces oxidative stress through the p53/SLC7A11/GPX4 axis, triggering ferroptosis and apoptosis in human osteosarcoma cells [29].

Our *in vitro* experiments demonstrated a significant reduction in mitochondrial membrane potential and a marked increase in ROS levels upon RPTS administration. *In vitro* and *in vivo* experiments focusing on ferroptosis-related proteins showed that RPTS administration significantly upregulated p53 protein expression while down-regulating GPX4 and SLC7A11 protein expression. Repeating these experiments with combined RPTS and Fer-1 administration

Journal of
BIOLOGICAL REGULATORS
and Homeostatic Agents

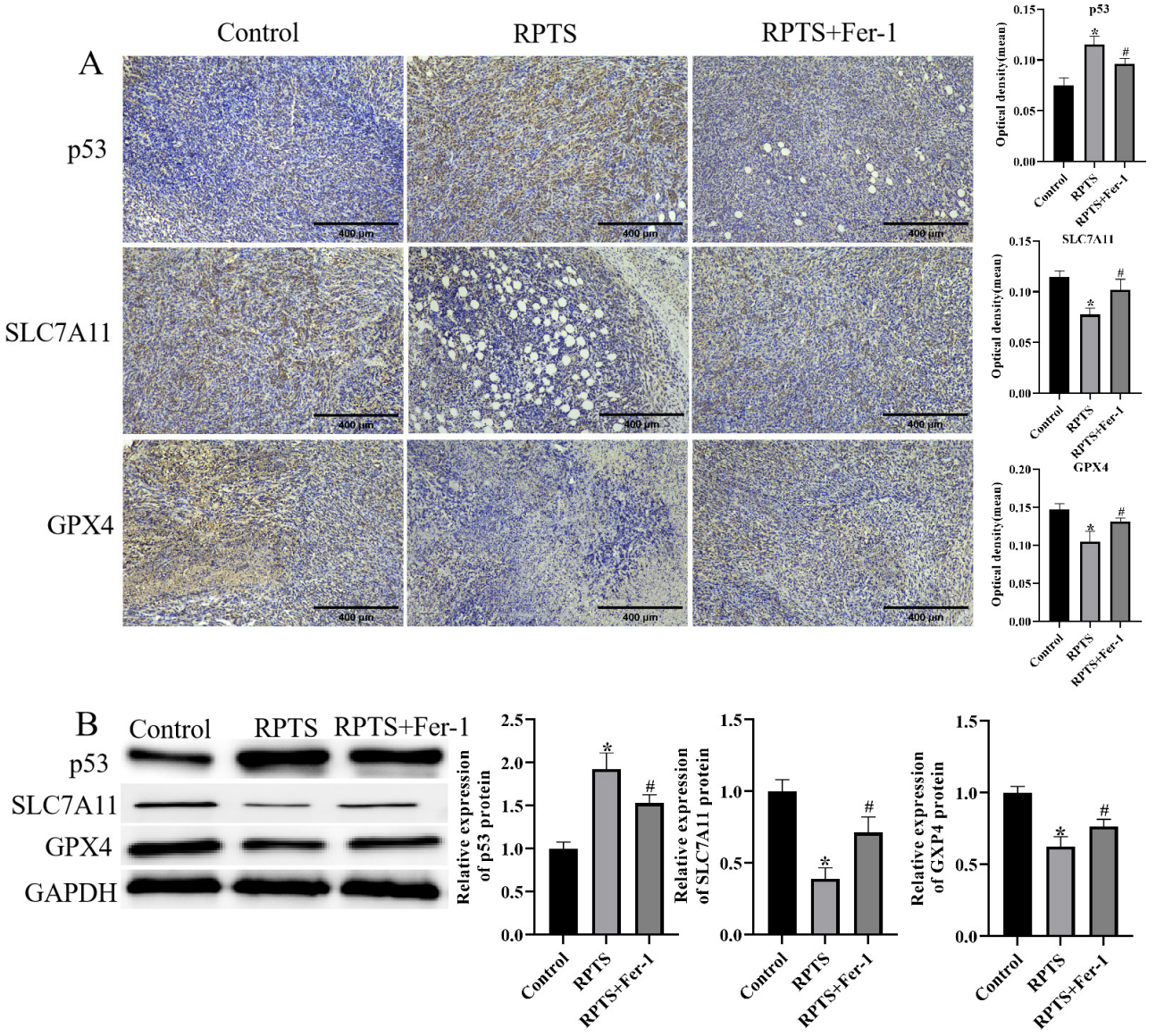

Fig. 6. Effects of RPTS on the expression levels of ferroptosis-related proteins p53, SLC7A11, and GPX4 in tumor tissues. (A) Analysis of ferroptosis-related protein expression levels using immunohistochemistry (scale bar = 400 μm). (B) Analysis of ferroptosis-related protein expression levels using western blotting. $^{*}p < 0.05$ vs Control, $^{\#}p < 0.05$ vs RPTS. n = 3.

revealed that the addition of Fer-1 significantly reversed the previously observed effects. These findings suggest that RPTS may induce ferroptosis in osteosarcoma cells or tissues through the p53/SLC7A11/GPX4 axis.

Moreover, dexamethasone administration has been reported to significantly reduce intracellular GSH levels, increase MDA and ROS levels in MC3T3-E1 cells, and induce ferroptosis through the p53/SLC7A11/GPX4 axis. However, SLC7A11 overexpression and the use of Fer-1 reversed dexamethasone-induced ferroptosis in MC3T3 cells [30]. Similarly, Shi *et al.* [31] conducted a study revealing that Tirapazamine (TPZ) exerts inhibitory effects on the proliferation of osteosarcoma cells by inducing ferroptosis. Interestingly, SLC7A11 overexpression restored the inhibitory capacity of TPZ to proliferation and migration of osteosarcoma cells. Our study demonstrated that SLC7A11 overexpression significantly increased cell proliferation and migration ability, decreased ROS levels, increased GPX4 expression, and decreased p53 expression in cells. These findings suggest that osteosarcoma cells experience reduced oxidative stress, and SLC7A11 overexpression rescues RPTS-induced ferroptosis in 143B cells. This implies that the mechanism of RPTS inhibition of osteosarcoma may involve decreased SLC7A11 expression.

This study unveils the potential of RPTS in osteosarcoma treatment, especially in inducing ferroptosis and modulating the EMT process. However, certain limitations persist. Despite RPTS demonstrating the ability to induce ferroptosis, its molecular mechanism remains incompletely elucidated. SLC7A11 overexpression attenuated the effect

of RPTS on ferroptosis, suggesting SLC7A11 as a potential key target. Furthermore, the EMT process, closely related to tumor invasion and recurrence, was inhibited by RPTS in this study, suggesting that it may represent another crucial target. Clinical validation is pivotal for advancing RPTS application, yet sufficient clinical data are lacking, necessitating further validation in humans. Moreover, the observations from this study are short-term, warranting additional long-term investigations to assess therapeutic effects. Future studies should validate these findings with prolonged clinical observations to comprehensively evaluate their therapeutic potential. Therefore, efforts should persist in unraveling the mechanism of action of RPTS, facilitating its clinical translation, and refining therapeutic strategies to optimize its efficacy.

Conclusion

In summary, RPTS induced ferroptosis in osteosarcoma by suppressing SLC7A11 expression and regulated cell viability, proliferation, apoptosis, migration, and the EMT process, indicating its inhibitory effect on osteosarcoma. This offers further insight into the role of ferroptosis in cancer therapy. However, the precise mechanism of action of RPTS still requires more in-depth investigations. Moreover, additional clinical studies are warranted to determine the potential application prospects of RPTS in the treatment of osteosarcoma.

Availability of Data and Materials

The datas used or analyzed during the current study are available from the corresponding author.

Author Contributions

QT conceived and designed the research study, acquired and analyzed the data, and wrote the initial draft of the manuscript. DY provided technical support for the acquisition and analysis of the data, performed statistical analysis, and contributed to the interpretation of the data and the manuscript revisions. QT and DY provided expertise in the field of study, contributed to the interpretation of the data, and critically revised the manuscript for important intellectual content. Both authors have read and approved the final manuscript, and have participated sufficiently in the work to take public responsibility for appropriate portions of the content.

Ethics Approval and Consent to Participate

This study was approved by the Ethics Committee of The Affiliated Children's Hospital of Xiangya School of Medicine (XY20237767).

Acknowledgment

Not applicable.

Funding

This work was supported by Opening Fundings of Hunan Provincial Key Laboratory of Pediatric Orthopedics (2023TP1019), Science and Technology Project of Furong Laboratory (2023SK2111), Hunan Provincial Clinical Medical Research Center for Pediatric Limb Deformities (2019SK4006), Sehan University Research Fund in 2024.

Conflict of Interest

The authors declare no conflict of interest.

Supplementary Material

Supplementary material associated with this article can be found, in the online version, at https://doi.org/10.23812/j.biol.regul.homeost.agents.20243806.417.

References

[1] Marko TA, Diessner BJ, Spector LG. Prevalence of Metastasis at Diagnosis of Osteosarcoma: An International Comparison. Pediatric Blood & Cancer. 2016; 63: 1006–1011.

[2] Friebele JC, Peck J, Pan X, Abdel-Rasoul M, Mayerson JL. Osteosarcoma: A Meta-Analysis and Review of the Literature. American Journal of Orthopedics (Belle Mead, N.J.). 2015; 44: 547–553.

[3] Ren J, Xu YF, Kuang TH, Chen J, Liu YX. Survival analysis of 104 cases of osteosarcoma with lung metastases. Zhonghua Zhong Liu Za Zhi [Chinese Journal of Oncology]. 2017; 39: 263–268.

[4] Benjamin RS. Adjuvant and Neoadjuvant Chemotherapy for Osteosarcoma: A Historical Perspective. Advances in Experimental Medicine and Biology. 2020; 1257: 1–10.

[5] Zhao SJ, Jiang YQ, Xu NW, Li Q, Zhang Q, Wang SY, *et al*. SPARCL1 suppresses osteosarcoma metastasis and recruits macrophages by activation of canonical WNT/β-catenin signaling through stabilization of the WNT-receptor complex. Oncogene. 2018; 37: 1049–1061.

[6] Sun Y, Jiang X, Lu Y, Zhu J, Yu L, Ma B, *et al*. Oridonin prevents epithelial-mesenchymal transition and TGF-β1-induced epithelial-mesenchymal transition by inhibiting TGF-β1/Smad2/3 in osteosarcoma. Chemico-biological Interactions. 2018; 296: 57–64.

[7] Gong H, Tao Y, Xiao S, Li X, Fang K, Wen J, *et al*. Identification of an EMT-related gene-based prognostic signature in osteosarcoma. Cancer Medicine. 2023; 12: 12912–12928.

[8] Mittal V. Epithelial Mesenchymal Transition in Tumor Metastasis. Annual Review of Pathology. 2018; 13: 395–412.

[9] Xie Y, Hou W, Song X, Yu Y, Huang J, Sun X, *et al*. Ferroptosis: process and function. Cell Death and Differentiation. 2016; 23: 369–379.

[10] Koppula P, Zhuang L, Gan B. Cystine transporter SLC7A11/xCT in cancer: ferroptosis, nutrient dependency, and cancer therapy. Protein & Cell. 2021; 12: 599–620.

[11] Luo Y, Gao X, Zou L, Lei M, Feng J, Hu Z. Bavachin Induces

Journal of
BIOLOGICAL REGULATORS
and Homeostatic Agents

Ferroptosis through the STAT3/P53/SLC7A11 Axis in Osteosarcoma Cells. Oxidative Medicine and Cellular Longevity. 2021; 2021: 1783485.

[12] Yuan S, Wei C, Liu G, Zhang L, Li J, Li L, *et al*. Sorafenib attenuates liver fibrosis by triggering hepatic stellate cell ferroptosis via HIF-1α/SLC7A11 pathway. Cell Proliferation. 2022; 55: e13158.

[13] Liu ST, Yu H, HouAJ, ManWJ, Zhang JX, Wang S, *et al*. A review of the pharmacology, application, ethnopharmacology, phytochemistry, quality control, processing, toxicology, and pharmacokineticsof Paridis Rhizoma. World Journal of Traditional Chinese Medicine. 2022; 8: 21–49.

[14] Zhao L, Peng P, Feng P, Yi SY. Mechanism Study on Rhodiolae Saponin Inducing Ferroptosis in Lung Cancer Cells via the JNK/p53 Pathway. Practical Journal of Cancer. 2023; 38: 713–717.

[15] Li X, Li D, Gao X, Shan Y, Xue J. Mechanism of Rhodiolae Saponin-induced Ferroptosis in Triple-Negative Breast Cancer Cells via the p53/SLC7A11 Signaling Axis. Journal of Chinese PLA Medical Journal. 2023; 48: 58–63.

[16] Lu KH, Chen PN, Hsieh YH, Lin CY, Cheng FY, Chiu PC, *et al*. 3-Hydroxyflavone inhibits human osteosarcoma U2OS and 143B cells metastasis by affecting EMT and repressing u-PA/MMP-2 via FAK-Src to MEK/ERK and RhoA/MLC2 pathways and reduces 143B tumor growth in vivo. Food and Chemical Toxicology: an International Journal Published for the British Industrial Biological Research Association. 2016; 97: 177–186.

[17] Jiang S, Zhou F, Zhang Y, Zhou W, Zhu L, Zhang M, *et al*. Identification of tumorigenicity-associated genes in osteosarcoma cell lines based on bioinformatic analysis and experimental validation. Journal of Cancer. 2020; 11: 3623–3633.

[18] Yang Z, Li X, Han W, Lu X, Jin S, Yang W, *et al*. Galangin suppresses human osteosarcoma cells: An exploration of its underlying mechanism. Oncology Reports. 2017; 37: 435–441.

[19] Lin H, Hao Y, Wan X, He J, Tong Y. Baicalein inhibits cell development, metastasis and EMT and induces apoptosis by regulating ERK signaling pathway in osteosarcoma. Journal of Receptor and Signal Transduction Research. 2020; 40: 49–57.

[20] Li J, Jia J, Zhu W, Chen J, Zheng Q, Li D. Therapeutic effects on cancer of the active ingredients in rhizoma paridis. Frontiers in Pharmacology. 2023; 14: 1095786.

[21] Labernadie A, Kato T, Brugués A, Serra-Picamal X, Derzsi S, Arwert E, *et al*. A mechanically active heterotypic E-cadherin/N-cadherin adhesion enables fibroblasts to drive cancer cell invasion. Nature Cell Biology. 2017; 19: 224–237.

[22] De Santis MC, Gulluni F, Campa CC, Martini M, Hirsch E. Targeting PI3K signaling in cancer: Challenges and advances. Biochimica et Biophysica Acta. Reviews on Cancer. 2019; 1871: 361–366.

[23] Fresno Vara JA, Casado E, de Castro J, Cejas P, Belda-Iniesta C, González-Barón M. PI3K/Akt signalling pathway and cancer. Cancer Treatment Reviews. 2004; 30: 193–204.

[24] Mondal S, Adhikari N, Banerjee S, Amin SA, Jha T. Corrigendum to "Matrix metalloproteinase-9 (MMP-9) and its inhibitors in cancer: A minireview" [Eur. J. Med. Chem. 194 (2020) 112260]. European Journal of Medicinal Chemistry. 2020; 205: 112642.

[25] Imai H, Matsuoka M, Kumagai T, Sakamoto T, Koumura T. Lipid Peroxidation-Dependent Cell Death Regulated by GPx4 and Ferroptosis. Current Topics in Microbiology and Immunology. 2017; 403: 143–170.

[26] Chen X, Li J, Kang R, Klionsky DJ, Tang D. Ferroptosis: machinery and regulation. Autophagy. 2021; 17: 2054–2081.

[27] Jiang L, Kon N, Li T, Wang SJ, Su T, Hibshoosh H, *et al*. Ferroptosis as a p53-mediated activity during tumour suppression. Nature. 2015; 520: 57–62.

[28] Lin H, Chen X, Zhang C, Yang T, Deng Z, Song Y, *et al*. EF24 induces ferroptosis in osteosarcoma cells through HMOX1. Biomedicine & Pharmacotherapy. 2021; 136: 111202.

[29] Liu Z, Wang X, Li J, Yang X, Huang J, Ji C, *et al*. Gambogenic acid induces cell death in human osteosarcoma through altering iron metabolism, disturbing the redox balance, and activating the P53 signaling pathway. Chemico-biological Interactions. 2023; 382: 110602.

[30] Sun F, Zhou JL, Liu ZL, Jiang ZW, Peng H. Dexamethasone induces ferroptosis via P53/SLC7A11/GPX4 pathway in glucocorticoid-induced osteonecrosis of the femoral head. Biochemical and Biophysical Research Communications. 2022; 602: 149–155.

[31] Shi Y, Gong M, Deng Z, Liu H, Chang Y, Yang Z, *et al*. Tirapazamine suppress osteosarcoma cells in part through SLC7A11 mediated ferroptosis. Biochemical and Biophysical Research Communications. 2021; 567: 118–124.